Ballistic One-Dimensional InAs Nanowire Cross-Junction Interconnects

Johannes Gooth,*,[†] Mattias Borg,[†] Heinz Schmid,[†] Vanessa Schaller,[†] Stephan Wirths,[†] Kirsten Moselund,[†] Mathieu Luisier,[‡] Siegfried Karg,[†] and Heike Riel*,[†]

[†]IBM Research — Zurich, Säumerstrasse 4, 8803 Rüschlikon, Switzerland
[‡]ETH Zurich, Integrated Systems Laboratory, Gloriastrasse 35, 8092 Zurich, Switzerland

S Supporting Information

ABSTRACT: Coherent interconnection of quantum bits remains an ongoing challenge in quantum information technology. Envisioned hardware to achieve this goal is based on semiconductor nanowire (NW) circuits, comprising individual NW devices that are linked through ballistic interconnects. However, maintaining the sensitive ballistic conduction and confinement conditions across NW intersections is a nontrivial problem. Here, we go beyond the characterization of a single NW device and demonstrate ballistic one-dimensional (1D) quantum transport in InAs NW cross-junctions, monolithically integrated on Si. Characteristic 1D conductance plateaus are resolved in field-effect measurements across up to four NW-junctions in series. The 1D ballistic transport and sub-band splitting is preserved for both crossing-directions. We show that the 1D modes of a single injection terminal can be distributed into multiple NW branches. We believe that NW cross-junctions are well-suited as cross-directional communication links for the reliable transfer of quantum information as required for quantum computational systems.

KEYWORDS: Nanowire, conductance quantization, quantum network, ballistic transport
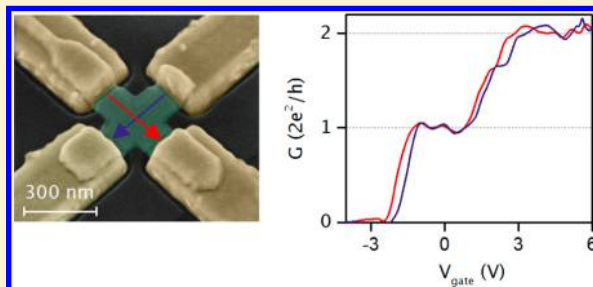
Exercising the full power of quantum information technology requires systems that maintain ballistic charge transport across many functional parts and connections. Compared to the linear increase in classically connected devices, the accessible state space in a system of full quantum connectivity increases exponentially with coherent constitutes, whereas long-range interactions provide instantaneous control on the encoded information.[1] Furthermore, nonlocal correlations enable one to store data globally, protecting it from local perturbations.[2,3] This makes quantum networks particularly interesting for communication, computation, and metrology. A possible physical implementation of that kind is a semiconductor nanowire (NW) network,[3] comprising individual NW devices that are coupled by ballistic interconnects. The most distinct applications of these one-dimensional (1D) networks would be in quantum computing based on Gatemons,[4,5] Majorana Fermions,[6−9] Parafermions[2,10] and Cooper pair splitters.[11−13] But they could also find potential applications in spintronic components,[14] ballistic transistors[15] and nonlinear circuit elements.[16] Electrical transport experiments on single III−V semiconducting NW channels have recently given direct evidence of 1D confined ballistic electron transport through the observation of quantized conductance plateaus.[17−25] Each plateau scales on integer multiples of $G_0 = 2e^2/h$, corresponding to the (de-) population of a single 1D mode with e denoting the electron charge and h being the Planck's constant. Moreover, spin qubit manipulation,[26]

Gatemon operation,[4] and the existence of Majorana Fermion quasiparticles,[6−9] that is, the building blocks of topological quantum computing, have been demonstrated. However, despite continuous progress in material growth it has proven very challenging to link individual NWs such that their 1D quantum nature translates into more complex networks; suppressing scattering is key. Therefore, electronic 1D quantum states can not be transmitted through conventional metallic interconnects. Reliable transfer of quantum information imposes stringent requirements on the connecting component to maintain the coherence of the 1D states.[27,28] The most basic proposed scheme for such an interconnection is a NW cross-junctions. Partially ballistic transport in top-down fabricated InGaAs[29] NW cross junction up to room temperature, tunable via gate voltage, has recently been reported and similar performance has been achieved in III-nitride[30] heterostructure-NW-crosses. Still, the observation of plateau-like 1D conductance quantization in such NW cross-junctions has been elusive so far in part because $In_xGa_{1−x}As$ and III-nitride exhibit relatively high effective masses. Another recently developed promising approach to enable ballistic 1D transport is within multiterminal NW junctions focused on either
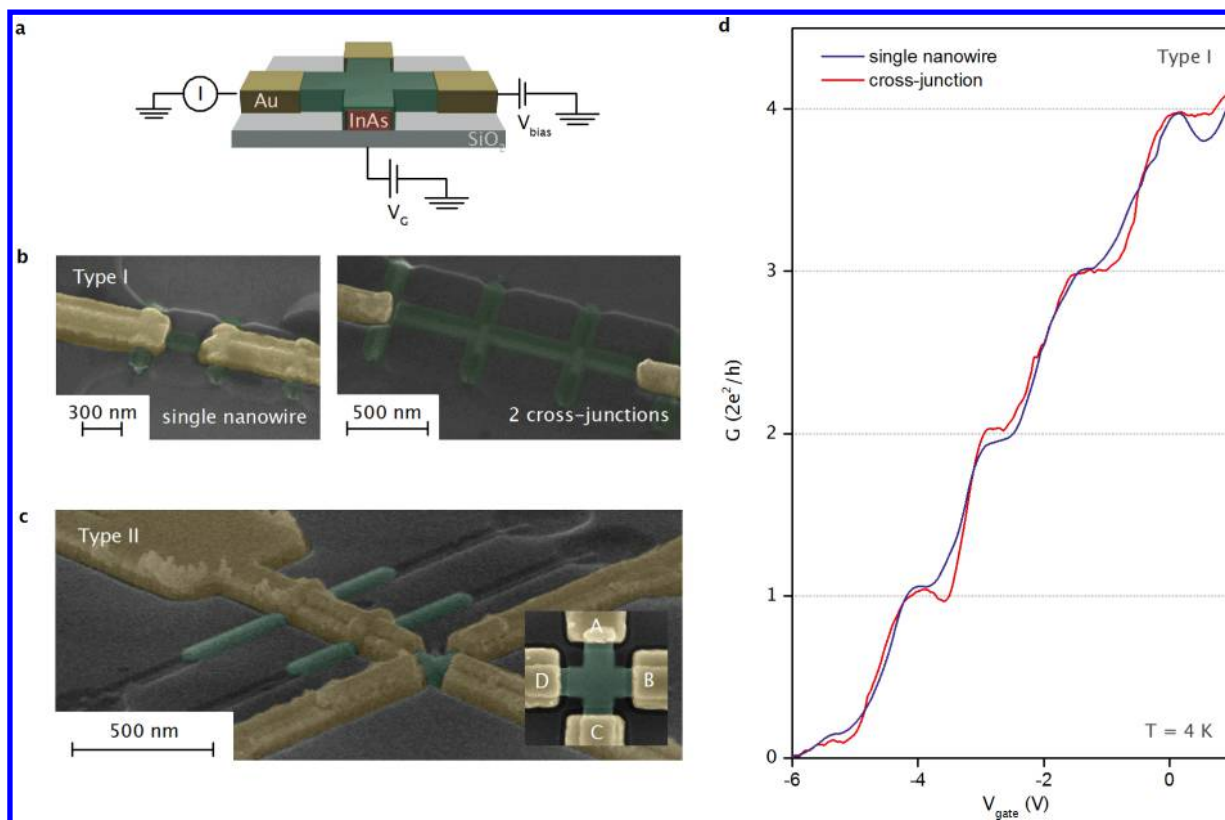
Figure 1. One-dimensional conductance quantization in InAs NW cross-junctions. (a) Schematic of the measurement device. Metallic probes (yellow) are connected to an InAs NW cross junction (red), covered by a protective oxide template (green). The current I out at one terminal in response to a bias voltage V_{bias} is measured as a function of gate voltage V_{gate}. (b) False-colored SEM image (color code above) of a type I device with a single NW (left) and two cross sections (right). The side-terminals are not contacted, but the longitudinal channel is equipped with two metallic terminals. The NWs cross-section is 25 nm × 50 nm and the gate oxide is 150 nm thick. (c) Tilted SEM view of a device of type II. Inset: SEM top view of the same device. All terminals of the cross-junction are connected by metal electrodes. The distance between contacts A and C as well as between B and D is 300 nm. The cross-section of the NW terminals is 20 nm × 50 nm. The gate oxide is 300 nm thick. (d) Electrical conductance $G = V_{bias}/I$ of a single NW (blue) and a NW cross-junction (red) as a function of gate voltage at 4 K, both of type II with channel lengths of 300 and 800 nm, respectively. The individual traces are corrected for the contact resistance. Both devices exhibit quantized 1D conductance plateaus.

depositing catalysts particles on already grown NWs, followed by a second growth step,[28,31] or by merging NWs in situ.[27,32,33] Although 1D quantization in these InAs[27,32,34] and InSb[28] devices should in principle be observable, current multiterminal NW devices suffer from defects and geometry issues due to limited control about positions, size, and shape at the intersection. Such methods are also difficult to scale up to larger networks. The transport in NW devices is very sensitive to the surface quality and therefore special care must be taken regarding passivation and protection. Consequently, a major step toward the technological implementation of NW-based quantum components is to combine single NWs and ballistic cross-junction interconnects with precise control of shape and surface quality, as well as to provide first demonstration of 1D quantum transport in these systems.

In this work, we have fabricated InAs NW cross-junctions, using template-assisted selective epitaxy (TASE),[35−37] providing geometric control and intrinsic surface protection through a SiO2 template. The 1D quantum transport is maintained over four gated NW cross junctions in series. Length-dependent studies reveal ballistic transport over distances as far as 800 nm and quasi-ballistic transport with a mean free path of (930 ± 50) nm in longer InAs NW channels at 4 K. We show that the transport features are independent of crossing-direction along the [110]-axis of the InAs crystal and that the 1D modes of a

single injection terminal can be distributed into multiple NW branches. This demonstrates that the implementation of single ballistic 1D NWs into complex network architectures is possible. The applied fabrication method is scalable to larger wafer size and fully compatible with main-stream silicon technology, providing a foundation for the development of NW-based quantum electronics.

The devices are prepared using the TASE process flow (see Supporting Information (SI) for details). III−V material is grown in prepatterned SiO2 templates that define the geometry and layout of the NW structure, here single NWs and NW cross-junctions. This allows for controlled placement and intentional branching of the NW devices. Metal−organic chemical vapor deposition (MOCVD) is then used to epitaxially deposit InAs within the templates from (100) Si seeds. The growth parameters are chosen such that each individual branch is pointing in the (110)-axis of the InAs crystal. However, we note that the TASE method permits the growth of nanostructures in any crystal direction in principle. A global back gate allows the control of the Fermi energy E_F during the transport measurements. Evaporated metal electrodes act as source-drain contacts to measure the current response I to a voltage bias V_{bias} (Figure 1a). To solely obtain the conductance of the NW channels, all data shown is corrected for series resistances of (6.7 ± 0.4) kΩ (SI Figure 3),
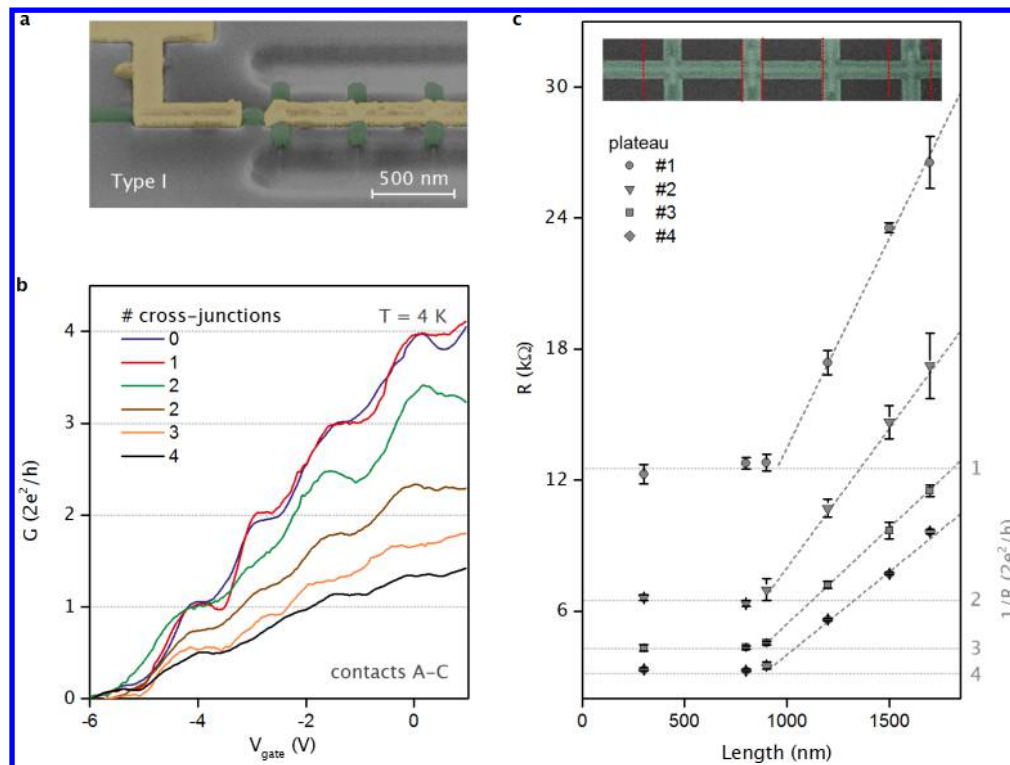
Figure 2. The 1D quantum transport across multiple NW junctions. (a) False-colored SEM image of a device with 0 cross-junctions. Six similar devices have been investigated but with different distance (length) between the left and the right contacts from 300 to 1700 nm. (b) $G–V_{gate}$ curves for various numbers of cross-junctions in the transport channel (l = 300 nm, blue; l = 800 nm, red; l = 900 nm, green; l = 1200 nm, brown; l = 1500 nm, orange; l = 1700 nm, black). On all curves, the same average contact resistance of 6.7 kΩ has been subtracted. (c) Experimental plateau resistance (symbols) as a function of channel length l. The values are obtained by averaging the data in (b) over the full width at half-maximum of the minima of the transconductance (SI Figure 6). The error reflects the standard deviation. The red dotted lines in the SEM inset mark the position of the right contact relative to the position of the left contact that corresponds L = 0 at the bottom axis. Up to 800 nm channel length, the devices remain ballistic, independent of the number of cross-junctions in the transport channel. Mean free paths of $\lambda = (930 \pm 50)$ nm are obtained from linear fits in the quasi-ballistic regime (lines) of $R = G_0^{-1}(1 + l/\lambda)$.

accounting for the contacts and leads of the devices. Please note that the template is only removed at the points of electrical contacts, providing in situ passivation of the NW surface along the transport channels. Data for two types of InAs NW devices are presented that we prepared on two different wafers: Type I devices (Figure 1b) exhibit multiple cross junctions between a two-terminal electrode configuration. The NW cross-section is 28 nm × 40 nm and the gate-oxide is 150 nm thick. Type II devices (Figure 1c) exhibit a single junction, where each terminal is contacted to a metal electrode. The spacing between opposite electrodes is 300 nm and the NW cross-section is 20 nm × 50 nm. The gate SiO_2 oxide is 300 nm thick. Of the 34 devices investigated, 30 show well-defined conductance plateaus (yield >85%). The devices are randomly distributed over (2 cm × 2 cm) large chips. There is no difference in yield between type I and type II devices. The Hall mobility of the template-protected devices at room temperature is 6200 cm^2 V^{-1} s^{-1} (SI Figure 4), similar to nonprotected devices with 5400 cm^2 V^{-1} s^{-1}.[35] However, when the SiO_2 template is removed, the conductance plateaus at 4 K are suppressed (SI Figure 5). Instead, oscillations occur that indicate the formation of random coulomb barriers due to impurities and trapped charges at the surface.[38]

First, we verify that TASE-grown single InAs NWs with no side arms attached exhibit ballistic 1D quantum transport (left panel of Figure 1 b). This is done by performing conductance measurements as a function of gate voltage V_{gate} at a fixed bias

of V_{bias} = 1 mV on a type I device and T = 4 K. As shown in Figure 1d, we observe conductance plateaus at integer multiples of G_0, consistent with ballistic 1D-confined charge transport. Quantum transport in single NWs has been studied in detail and such conductance steps are considered as hallmark for 1D sub-bands.[17,22−24]

Next, we turn to investigate the quantum transport in a NW cross-junction with the same channel profile (type I) as the single NW, but with two side arms attached at an intersection. Again, a conductance measurement is employed as a function of V_{gate} at fixed bias voltage. Note that for now the two side arms are kept floating. In principle, a cross-junction poses a potential source of scattering, detrimental to the transmission of 1D modes. Geometric, electronic, and material defects at the intersection can modify the injected electron beam, distributing the charge carriers from the source terminal into all attached NWs. Narrowing the drain terminal, may cause reflection[39] as well as subsequent scrambling effects[39] and the locally reshaped confinement potential at the crossing-point could lead to unintentional Coulomb blockades.[38] In any case, the 1D transport characteristic would be suppressed, compared to a single NW channel. However, as exemplified in Figure 1d, the $G–V_{gate}$ curves of the cross-junctions match the single NW-trace very well and we observe the same distinct features of ballistic 1D transport. The NW intersection is sufficiently transparent to allow for unhindered transmission of 1D modes.
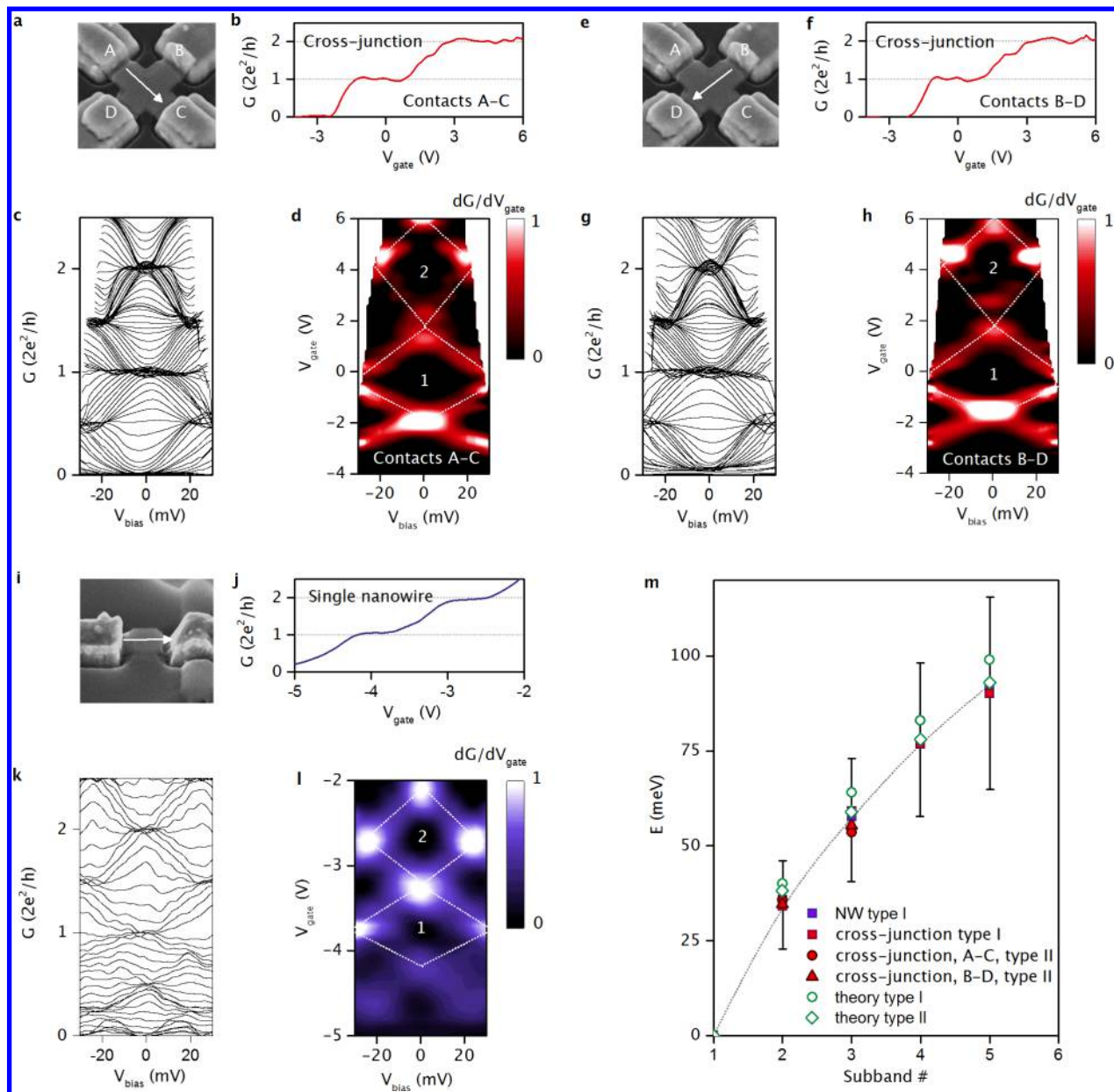
Figure 3. Bias spectroscopy of the 1D sub-band structure at 4 K. (a−d) Two-terminal measurements on a type II cross-junction between contacts A−C (B−D are kept floating). (e−h) Two-terminal measurements on a type II cross-junction between contacts B−D (A−C are kept floating). (i−l) Two-terminal measurements on a type I single NW. (a,e,i) SEM image of the investigated device and scheme of the transport direction. (b,f,j) G−V_{gate} sweep at constant $V_{bias} = 1$ mV show similar 1D conductance steps for both crossing directions of the junction and the single NW. (c,g,k) Bias-corrected differential conductance $G = dI/dV_{bias}$ as a function of V_{bias} and V_{gate}. Plateaus of multiple integer of G_0 around zero V_{bias} and half-plateaus of intermediate values at high V_{bias} are observed for all measurement configurations investigated. (d,h,l) The corresponding transconductance $g = dG/dV_{bias}$ reveals diamond-like structures whose width directly reflects the distance between the individual sub-bands. (m) Experimentally extracted position of the 1D sub-bands relative to the first mode. Because type I and type II devices exhibit very similar cross sections, their sub-band spacing matches within the measurement error (filled symbols), estimated from the average of the negative and the positive biases. For comparison, the corresponding theoretical values (green open symbols) are calculated using an infinite-potential-well-model.

Consequently, the transport across multiple NW interconnects should not be dominated by the number of nodes in the transport channel but rather by the mean free path λ of charge carriers determined by the channel between the junctions. A crucial test is then to evaluate the height of the conductance plateaus as a function of channel length l in the quasi-ballistic limit. For a λ-limited 1D system, the inverse conductance value of the nth plateau G_n^{-1} scales linearly with l as $G_n^{-1} = G_{n,0}^{-1}(1 + l/\lambda)$,[18,40] where $G_{n,0}$ denotes the fully ballistic conductance value of the nth plateau $n\cdot 2e^2/h$. We therefore prepare NW

devices of type I with various length and number of nodes in the transport channel (Figure 2a). The measured conductance is shown in Figure 2b. Extracting the height of the plateaus as a function of channel length (Figure 2c), fully ballistic transport up to $l = 800$ nm across one junction is obtained. The plateau resistance G_n^{-1} of longer channels increases linear with increasing l as expected for a single NW channel and crucially not with the number of cross-junctions (see SI Figure 7 for cross-check). Linear fits to our measurement data reveal a mean free path of (930 ± 50) nm. Importantly, as seen in Figure 3b,f,

the 1D ballistic transport is independent of crossing direction, indicating ballistic cross-directional 1D transport.

To further exclude that the intersections of the crossed NWs affect the quantum transport, we perform bias spectroscopy, which provides direct insights into the energy structure of the devices. Comparing the spectroscopic cross-directional data of a type II junction (Figure 3a−h) with that of a single NW of type I (Figure 3i−l), we do not obtain any significant differences between their energy subtexture. Both devices reveal similar quantization on multiple integers of G_0, at low bias voltage (V_{bias}) that evolves into half-plateaus of intermediate values at high V_{bias} (Figure 3c,g,k). Such half-plateaus arise when the two chemical potentials in source and drain contacts occupy different sub-bands. As most apparent in the transconductance $g = dG/dV_{gate}$ (Figure 3d,h,l), diamond-like structures are formed, which tips reflect the spacing between the corresponding sub-bands i and j: $\Delta\epsilon_{i,j} = eV_{bias,tip}$. Comparing the experimentally extracted sub-band position, relative to the first band, we find not only (1) the formation of conductance plateaus but also (2) that the spacing of the energy levels is independent of the transport direction across the junction and (3) that the energy levels trace the sub-band-splitting of a single NW very well. Although the quantum confinement is expected to be size-dependent, the relatively similar size of the NW cross sections of type I (1120 nm^2) and II (1000 nm^2) allows for a quantitative comparison within the measurement error. In agreement with our previous study on single NWs, the sub-band spacing of the cross-junctions follows a simple infinite-potential-well model.[40] The NW junctions, hence, sustain ballistic transmission of 1D modes, when the side-arms attached are floating.

An important check for actual network applications is whether the 1D state transmission is robust under simultaneous cross-directional operation. Compared to the case with floating side arms, the potential landscape in the cross-junction may be locally distorted when the side arms are contacted, because of different lateral working biases that could distract the trajectory of the injected electrons. To verify this, a potential of +500 μV is applied to terminal A and B and a potential of −500 μV is symmetrically applied to terminal C and D (Figure 4a), thus sending ballistic charge carriers across from A to C and from B to C (see SI Figure 10 for a measurement scheme). As shown in Figure 4a, we observe that the current signal measured at the inputs (I_A, I_B) and outputs (I_C, I_D) of the device essentially follows the same step-functional shape as the signal transmitted with floating side arms with plateaus close to the expected values for $G_{n,0}$. We do observe a slight substructure on the plateaus, probably due to minor lateral quantum mechanical cross-talk. Despite the presence of stacking faults that run along the [111] direction of the crystal,[36] we do not observe an anisotropy in the transport of the cross-junction, indicating a uniform electronic material. These results are consistent with our previous study at room-temperature.[35] In contrast, previous reports on predominantly zinc blende InAs NWs with extended wurtzite segments have shown signatures of barriers in the electrical transport.[41] We believe that the relatively high density of one stacking fault per nanometer rather creates an effective band structure in our NW devices. Apparently, the NW cross-junctions allow for simultaneous cross-directional quantum information transfer.

Next, we test if the 1D modes from a single input terminal can be distributed into multiple NW branches. For this experiment I_B is also set to −500 μV. In this configuration, the
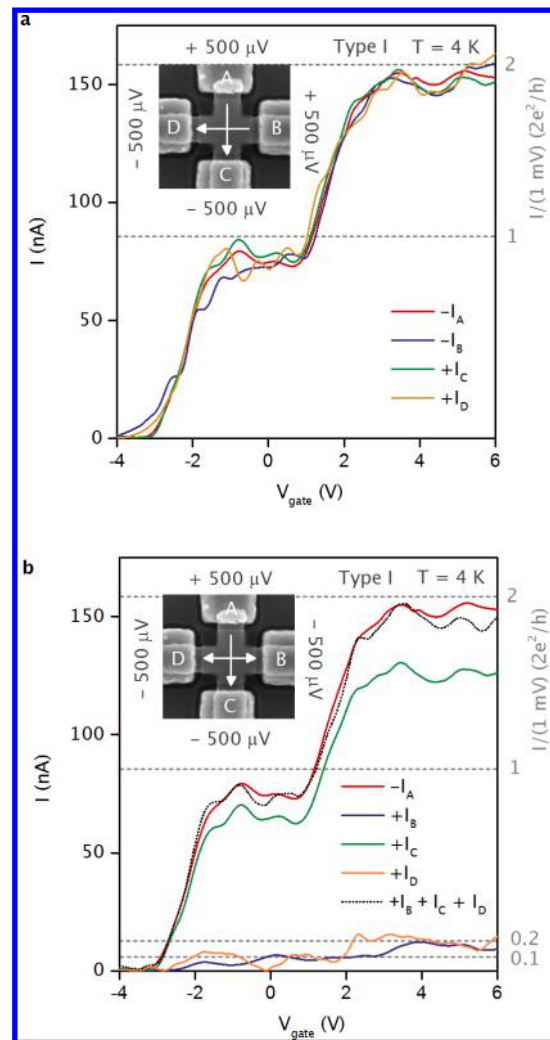
Figure 4. Four-terminal transport experiments on a type II NW cross-junction. The current signal at each terminal (I_A, I_B, I_C, I_D) is measured as response to the four-terminal voltage bias. The arrows in the insets mark the current flow direction. (a) Simultaneous-cross-directional operation is tested by applying +500 mV to terminal A and B, and −500 mV to terminal C and D. (b) Spreading of the 1D states from the input to all attached terminals is investigated by setting B also to −500 μV.

observed first and the second sub-band are still transmitted across the junction (Figure 4b) but the current signal measured at the output situated across the port of input (I_C) is suppressed. This is because around 20% of the input signal is transmitted into the lateral branches of the NW cross. The fraction of the signal that is transferred to these outputs (I_B, I_D) is almost symmetric and still carries the steplike 1D information on the input terminal, indicating scattering into the laterally attached terminals. This collimation effect is probably caused by a deformation of the potential profile by the lateral voltage loads,[42] compared to floating side-terminals. As dictated by charge conservation, the experimental data reveals $I_A = I_B + I_C + I_D$. The observed features are in qualitative agreement with quantum mechanical simulations of an InAs nanocross, for which details can be seen in the SI. This is an important cross-check, confirming the results and interpretation above. It also excludes that the observed quantization originates only from a local pinning point in the NW channel. Lateral voltages seem thus to enable the distribution of 1D modes from a single

injection terminal into complex NW networks. However, care must be taken during simultaneous cross-directional operation regarding ballistic cross-talk. The details of which will depend on the specific material, cross-section of the NW channel, shape of the corners. and angle between the NW branches, requiring further investigations.

We conclude that NW cross-junctions are well suited as cross-directional communication links for the reliable transfer of quantum information across ballistic 1D networks and thus for building a computational system that maintains quantum rules across multiple connected nodes. The advantage of the TASE method for quantum network design, compared to conventional NW grow techniques, are the precise control about placement, size, branching, scalability, and control about the crystal orientation of the individual branches. Moreover, TASE provides in situ surface passivation as well as the monolithic integration of III−V quantum networks on Si. The future experiments involving magneto-transport studies to investigate the g-factor of these 1D materials are anticipated. Apart from the ballistic transfer of 1D quantum states across a single node, we believe there is an important advantage in the option to connect several NW junctions in series. A system of quantum connectivity, as opposed to classical connectors in between functional parts, provides an exponentially larger state dimension for computation.

■ ASSOCIATED CONTENT

Ⓢ Supporting Information

The Supporting Information is available free of charge on the ACS Publications website at DOI: 10.1021/acs.nanolett.7b00400.

> State-of-the-art figure toward III−V quantum wire networks, a methods section, an analysis of the contact resistance, the estimation of the plateau-width of Figure 2c, the plateaus-height versus the number of NW cross-junctions in the transport channel, a comparison of the conductance quantization with and without template, room-temperature Hall data, the bias spectroscopy of type II devices, all current−voltage characteristics corresponding to the bias spectroscopies, and quantum mechanical simulations of a nanowire-cross-junction (PDF)

■ AUTHOR INFORMATION

Corresponding Authors

*E-mail: (J.G.) jog@zurich.ibm.com.
*E-mail: (H.R.) hei@zurich.ibm.com.

ORCID Ⓘ

Johannes Gooth: 0000-0002-4062-3232
Mattias Borg: 0000-0003-1217-369X
Heinz Schmid: 0000-0002-0228-4268

Author Contributions

J.G. and M.B. conceived the original idea for the study. M.B., H.S., and S.W. synthesized the InAs nanowires. M.B., V.S., and S.K. fabricated the NW devices. J.G. carried out the transport measurements with the help of V.S., J.G., M.B., and H.S., and T.M. analyzed the data. M.L performed the theoretical calculations. K.M. and H.R. supervised the project. All authors contributed to the interpretation of the data and to the writing of the manuscript.

■ REFERENCES

(1) Kimble, H. J. *Nature* **2008**, *453* (7198), 1023−1030.
(2) Hutter, A.; Loss, D. *Phys. Rev. B: Condens. Matter Mater. Phys.* **2016**, *93* (12), 125105.
(3) Alicea, J.; Oreg, Y.; Refael, G.; von Oppen, F.; Fisher, M. P. a. *Nat. Phys.* **2011**, *7* (5), 412−417.
(4) Casparis, L.; Larsen, T. W.; Olsen, M. S.; Kuemmeth, F.; Krogstrup, P.; Nygard, J.; Petersson, K. D.; Marcus, C. M. *Phys. Rev. Lett.* **2016**, *116* (15), 150505.
(5) Larsen, T. W.; Petersson, K. D.; Kuemmeth, F.; Jespersen, T. S.; Krogstrup, P.; Nygard, J.; Marcus, C. M. *Phys. Rev. Lett.* **2015**, *115* (12), 150505.
(6) Das, A.; Ronen, Y.; Most, Y.; Oreg, Y.; Heiblum, M.; Shtrikman, H. *Nat. Phys.* **2012**, *8* (12), 887−895.
(7) Albrecht, S. M.; Higginbotham, A. P.; Madsen, M.; Kuemmeth, F.; Jespersen, T. S.; Nygard, J.; Krogstrup, P.; Marcus, C. M. *Nature* **2016**, *531* (7593), 206−209.
(8) Deng, M. T.; Yu, C. L.; Huang, G. Y.; Larsson, M.; Caroff, P.; Xu, H. Q. *Nano Lett.* **2012**, *12* (12), 6414−6419.
(9) Mourik, V.; Zuo, K.; Frolov, S. M.; Plissard, S. R.; Bakkers, E. P. a. M.; Kouwenhoven, L. P. *Science* **2012**, *336* (6084), 1003−1007.
(10) Klinovaja, J.; Loss, D. *Phys. Rev. Lett.* **2014**, *112*, 24.
(11) Rokhinson, L. P.; Liu, X.; Furdyna, J. K. *Nat. Phys.* **2012**, *8* (11), 795−799.
(12) Hofstetter, L.; Csonka, S.; Nygard, J.; Schonenberger, C. *Nature* **2009**, *461* (7266), 960−963.
(13) Das, A.; Ronen, Y.; Heiblum, M.; Mahalu, D.; Kretinin, A. V.; Shtrikman, H. *Nat. Commun.* **2012**, *3*, 1165.
(14) Liang, D.; Gao, X. P. A. *Nano Lett.* **2012**, *12* (6), 3263−3267.
(15) Gilbert, M. J.; Banerjee, S. K. *IEEE Trans. Electron Devices* **2007**, *54* (4), 645−653.
(16) Stano, P.; Jacquod, P. *Phys. Rev. Lett.* **2011**, *106*, 20.
(17) Heedt, S.; Prost, W.; Schubert, J.; Grützmacher, D.; Schäpers, T. *Nano Lett.* **2016**, *16* (5), 3116−3123.
(18) Ford, A. C.; Kumar, S. B.; Kapadia, R.; Guo, J.; Javey, A. *Nano Lett.* **2012**, *12* (3), 1340−1343.
(19) Chuang, S.; Gao, Q.; Kapadia, R.; Ford, A. C.; Guo, J.; Javey, A. *Nano Lett.* **2013**, *13* (2), 555−558.
(20) Abay, S.; Persson, D.; Nilsson, H.; Xu, H. Q.; Fogelström, M.; Shumeiko, V.; Delsing, P. *Nano Lett.* **2013**, *13* (8), 3614−3617.
(21) Mensch, P.; Karg, S.; Schmidt, V.; Gotsmann, B.; Schmid, H.; Riel, H. *Appl. Phys. Lett.* **2015**, *106* (9), 093101.
(22) Heedt, S.; Manolescu, A.; Nemnes, G. A.; Prost, W.; Schubert, J.; Grützmacher, D.; Schäpers, T. *Nano Lett.* **2016**, *16* (7), 4569−4575.
(23) Kammhuber, J.; Cassidy, M. C.; Zhang, H.; Gül, Ö.; Pei, F.; de Moor, M. W. A.; Nijholt, B.; Watanabe, K.; Taniguchi, T.; Car, D.; Plissard, S. R.; Bakkers, E. P. A. M.; Kouwenhoven, L. P. *Nano Lett.* **2016**, *16* (6), 3482.
(24) Van Weperen, I.; Plissard, S. R.; Bakkers, E. P. A. M.; Frolov, S. M.; Kouwenhoven, L. P. *Nano Lett.* **2013**, *13* (2), 387−391.

(25) Zota, C. B.; Lindgren, D.; Wernersson, L.-E.; Lind, E. *ACS Nano* **2015**, *9* (10), 9892−9897.

(26) Petersson, K. D.; McFaul, L. W.; Schroer, M. D.; Jung, M.; Taylor, J. M.; Houck, a a; Petta, J. R. *Nature* **2012**, *490* (7420), 380−383.

(27) Heedt, S.; Vakulov, D.; Rieger, T.; Rosenbach, D.; Trellenkamp, S.; Grützmacher, D.; Lepsa, M. I.; SchäPers, T. *Adv. Electron. Mater.* **2016**, *2* (6), 2482−3486.

(28) Plissard, S. R.; van Weperen, I.; Car, D.; Verheijen, M. a; Immink, G. W. G.; Kammhuber, J.; Cornelissen, L. J.; Szombati, D. B.; Geresdi, A.; Frolov, S. M.; Kouwenhoven, L. P.; Bakkers, E. P. a M. *Nat. Nanotechnol.* **2013**, *8* (11), 859−864.

(29) Thathachary, A. V.; Agrawal, N.; Liu, L.; Datta, S. *Nano Lett.* **2014**, *14* (2), 626−633.

(30) Matioli, E.; Palacios, T. *Nano Lett.* **2015**, *15* (2), 1070−1075.

(31) Dick, K. A.; Deppert, K.; Karlsson, L. S.; Seifert, W.; Wallenberg, R.; Samuelson, L. *Nano Lett.* **2006**, *6* (12), 2842−2847.

(32) Rieger, T.; Rosenbach, D.; Vakulov, D.; Heedt, S.; SchäPers, T.; Grützmacher, D.; Lepsa, M. I. *Nano Lett.* **2016**, *16* (3), 1933−1941.

(33) Huang, Y.; Duan, X.; Wei, Q.; Lieber, C. M. *Science* **2001**, *291* (5504), 630−633.

(34) Suyatin, D. B.; Sun, J.; Fuhrer, A.; Wallin, D.; Fröberg, L. E.; Karlsson, L. S.; Maximov, I.; Wallenberg, L. R.; Samuelson, L.; Xu, H. Q. *Nano Lett.* **2008**, *8* (4), 1100−1104.

(35) Schmid, H.; Borg, M.; Moselund, K.; Gignac, L.; Breslin, C. M.; Bruley, J.; Cutaia, D.; Riel, H. *Appl. Phys. Lett.* **2015**, *106* (23), 233101.

(36) Borg, M.; Schmid, H.; Moselund, K. E.; Cutaia, D.; Riel, H. *J. Appl. Phys.* **2015**, *117*, 144303.

(37) Borg, M.; Schmid, H.; Moselund, K. E.; Signorello, G.; Gignac, L.; Bruley, J.; Breslin, C.; Das Kanungo, P.; Werner, P.; Riel, H. *Nano Lett.* **2014**, *14* (4), 1914−1920.

(38) Wu, P. M.; Gooth, J.; Zianni, X.; Svensson, S. F.; Gluschke, J. G.; Dick, K. A.; Thelander, C.; Nielsch, K.; Linke, H. *Nano Lett.* **2013**, *13* (9), 4080−4086.

(39) Beenakker, C. W. J.; Van Houten, H. *Phys. Rev. Lett.* **1989**, *63* (17), 1857−1860.

(40) Gooth, J.; Schaller, V.; Wirths, S.; Schmid, H.; Borg, M.; Bologna, N.; Karg, S.; Riel, H. *Appl. Phys. Lett.* **2017**, *110* (8), 083105.

(41) Thelander, C.; Caroff, P.; Plissard, S.; Dey, A. W.; Dick, K. A. *Nano Lett.* **2011**, *11*, 2424−2429.

(42) Molenkamp, L. W.; Staring, A. A. M.; Beenakker, C. W. J.; Eppenga, R.; Timmering, C. E.; Williamson, J. G.; Harmans, C. J. P. M.; Foxon, C. T. *Phys. Rev. B: Condens. Matter Mater. Phys.* **1990**, *41* (2), 1274−1277.